

# Accelerating Bayesian Optimization for Biological Sequence Design with Denoising Autoencoders

Samuel Stanton<sup>1</sup> Wesley Maddox<sup>1</sup> Nate Gruver<sup>2</sup> Phillip Maffettone<sup>3</sup> Emily Delaney<sup>3</sup>  
Peyton Greenside<sup>3</sup> Andrew Gordon Wilson<sup>1,2</sup>

## Abstract

Bayesian optimization is a gold standard for query-efficient continuous optimization. However, its adoption for drug and antibody sequence design has been hindered by the discrete, high-dimensional nature of the decision variables. We develop a new approach (LaMBO) which jointly trains a denoising autoencoder with a discriminative multi-task Gaussian process head, enabling gradient-based optimization of multi-objective acquisition functions in the latent space of the autoencoder. These acquisition functions allow LaMBO to balance the explore-exploit trade-off over multiple design rounds, and to balance objective tradeoffs by optimizing sequences at many different points on the Pareto frontier. We evaluate LaMBO on a small-molecule task based on the ZINC dataset and introduce a new large-molecule task targeting fluorescent proteins. In our experiments, LaMBO outperforms genetic optimizers and does not require a large pretraining corpus, demonstrating that Bayesian optimization is practical and effective for biological sequence design.

## 1. Introduction

Protein design is the process of creating new or improved protein structures for use as biomarkers, therapeutics, and other applications. Protein properties are difficult to predict directly from primary amino acid residue sequences, even for well-studied families. Obtaining new labels involves synthesizing sequences and observing their properties in a wet-lab, which can take weeks. As a result, protein design is naturally framed as an expensive black-box optimization (BBO) problem over a large discrete search space.

Recent work applying deep learning to biological tasks has primarily focused on learning structure, function, or a generative sequence model from a static, offline dataset (Rao et al., 2019; Jumper et al., 2021; Baek et al., 2021; Meier

<sup>1</sup>Center for Data Science, NYU, New York, USA <sup>2</sup>Courant Institute of Mathematical Sciences, NYU, New York, USA <sup>3</sup>BigHat Biosciences, San Mateo, CA, USA. Correspondence to: Samuel Stanton <ss13641@nyu.edu>.

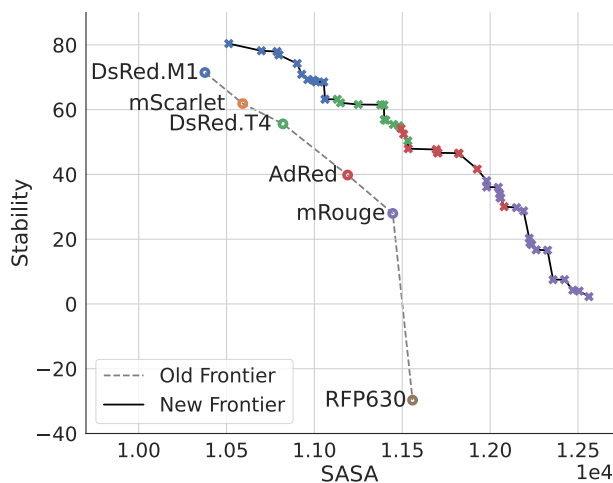


Figure 1. BayesOpt can be used to maximize the simulated folding stability ( $-dG$ ) and solvent-accessible surface area (SASA) of red-spectrum fluorescent proteins. Higher is better for both objectives. The starting proteins are shown as colored circles, with corresponding optimized offspring shown as crosses. Stability correlates with protein function (e.g. how long the protein can fluoresce) while SASA is a proxy for fluorescent intensity.

et al., 2021; Rives et al., 2021). When these models are used to select new sequences to synthesize, they are applied in a one-shot fashion, without accounting for future design rounds (Gligorijevic et al., 2021; Biswas et al., 2021). In the context of campaigns targeting novel families or fitness criteria it is important to account for model uncertainty to manage the exploration-exploitation tradeoff (O’Donoghue et al., 2018).

Bayesian optimization (BayesOpt) is a powerful class of BBO algorithms, explicitly designed to *coherently* reason about online decision-making based on incomplete information (e.g., Jones et al., 1998; Brochu et al., 2010; Frazier, 2018). BayesOpt balances the explore-exploit tradeoff in a principled way, relying on a probabilistic discriminative model to prioritize decisions with the highest potential payoff. At each decision point the discriminative model produces a posterior distribution over the hypothesis space of all functions the model can represent. The posterior formally represents the degree to which any particular hypothesis is consistent with the available data, given the model assumptions. To make a decision, BayesOpt optimizes for the best outcome as defined by an *acquisition function*, such as

expected improvement, or value of information, with each hypothesis contributing to the acquisition value in proportion to its posterior probability. BayesOpt is not merely philosophically appealing, it is provably a *no-regret* strategy under the right conditions (Srinivas et al., 2010).

Like many Bayesian methods, often the barriers hindering widespread adoption of BayesOpt are not conceptual, but *practical*. Protein design in particular is a natural application domain, but introduces multiple serious challenges. *Discrete, high-dimensional inputs*: a single protein is commonly represented as a sequence of hundreds of residues, each representing one of 20 possible amino acids. Even a relatively small protein with 200 residues (i.e. 200 decision variables) is one possibility out of  $20^{200} \approx 1.6 \times 10^{260}$ .<sup>1</sup> By contrast, conventional BayesOpt works best on problems with 10 or fewer continuous decision variables, due to the properties of standard kernels, and the availability of gradients to maximize the acquisition function. *Batched, multi-objective experiments*: because considerations including efficacy, toxicity, and yield must all be taken into account, protein design is inherently multi-objective. Furthermore proteins are synthesized and observed in batches, necessitating the use of more sophisticated acquisition functions than standard workhorses like expected improvement. *Data-scarcity*: wet-lab experimental data is expensive and challenging to collect, so it is rare to have large-scale datasets with labels for the exact target features of interest.

At the time of writing, no single BayesOpt method has been proposed to simultaneously address all of these challenges. As a result, previous methods have necessarily only been evaluated on very stylized tasks that fail to capture key characteristics of protein design problems. In this work we present **Latent Multi-Objective BayesOpt (LaMBO)** to address this deficiency. We also propose a novel simulated benchmark task to aid in the evaluation of current and future methods for ML-guided protein design. The task is constructed to more closely resemble protein design tasks than common open-source benchmarks for discrete sequence design. We preview our results applying LaMBO to this new task in Figure 1. We jointly maximize both the solvent-accessible surface area (SASA) and the stability (i.e.  $-dG$ , or the negative change in Gibbs free energy) of red-spectrum fluorescent proteins (RFPs) found in the open-source fp-Base dataset (Lambert, 2019). The original Pareto frontier derived from existing RFPs with known structure is shown as a dashed line. The new Pareto frontier discovered by LaMBO (shown as a solid line) is substantially superior, as it is characterized much more densely by new sequences that are Pareto improvements over their predecessors.

<sup>1</sup>For a sense of scale, with an estimated  $10^{80}$  atoms in our observable universe, enumerating  $10^{260}$  would be like counting atoms if every atom in our universe was itself a universe, and all the atoms in *those* universes were also universes.

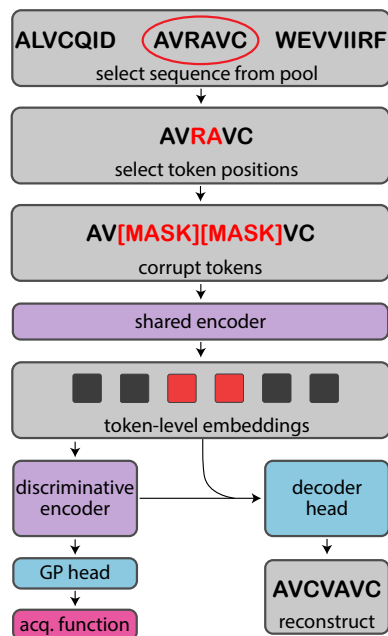


Figure 2. LaMBO with a non-autoregressive denoising autoencoder model: a shared, bidirectional encoder produces continuous token-level embeddings  $Z$  from corrupted input sequences, which are passed to a discriminative encoder to produce task-specific token-level embeddings  $Z'$ . A generative decoder head receives both  $Z$  and  $Z'$  as input, and a discriminative GP head pools  $Z'$  to predict the objective values. The GP head allows the use of principled acquisition functions to manage the explore-exploit tradeoff, and the decoder head allows LaMBO to follow the acquisition gradient in latent space when selecting new queries.

In short, our contributions include:

1. The LaMBO architecture (Figure 2) and training procedure, addressing the high-dimensional, multi-objective, data-scarce setting of protein design, through a novel combination of deep kernel learning (DKL) for supervised GP inference and non-autoregressive denoising autoencoders (DAEs) for unsupervised learning.
2. The LaMBO inner loop optimization routine, including a reliable initialization procedure which addresses pitfalls of multi-objective acquisition functions.
3. The introduction of a novel, well-motivated multi-objective benchmark task maximizing SASA and stability of red fluorescent proteins from fpBase.
4. Strong empirical results on a commonly-used small-molecule design task, as well as our newly proposed task, with comparisons to both genetic and latent optimization baselines.
5. We provide code at <https://github.com/samuelstanton/lambo>.

## 2. Preliminaries

In this section, we describe the discrete sequence design problem setting and briefly introduce BayesOpt.

### 2.1. Multi-Objective Sequence Design

We focus on unstructured discrete sequence design tasks. We begin by defining the input space,

$$\mathcal{X} = \bigtimes_{i=1}^t \mathcal{V},$$

where  $\mathcal{V}$  is an ordered, discrete vocabulary of  $v$  tokens,  $t$  is the max sequence length, and  $\times$  is the Cartesian product.  $\mathcal{V}$  includes a padding token to accommodate sequences of varying length. Because  $|\mathcal{X}| = |\mathcal{V}|^t$  is exponential in  $t$ ,  $\mathcal{X}$  becomes too large to enumerate quickly as the sequence length grows, even if  $|\mathcal{V}|$  is relatively small. As a result, sequence optimization usually starts with a library or pool of initial sequences (as shown at the top of Figure 2), which are modified to produce new candidate sequences. When posed in this way, the optimization problem is restructured into three nested decisions: (1) Choose a base sequence from the pool. (2) Choose which positions on the sequence to change. (3) Choose how the sequence will be changed at those positions.

We represent sequence design as a multi-objective optimization problem  $\min_{\mathbf{x} \in \mathcal{X}} (f_1(\mathbf{x}), \dots, f_k(\mathbf{x}))$ , where each  $f_i : \mathcal{X} \rightarrow \mathbb{R}$  is an expensive, black-box function of decision variables  $\mathbf{x} \in \mathcal{X}$ , and  $k$  is the number of objectives. Given two feasible solutions  $\mathbf{x}$  and  $\mathbf{x}'$ ,  $\mathbf{x}$  *dominates*  $\mathbf{x}'$  ( $\mathbf{x} > \mathbf{x}'$ ) if  $f_i(\mathbf{x}) \leq f_i(\mathbf{x}') \forall i \in \{1, \dots, k\}$ , and  $\exists i \in \{1, \dots, k\}$  s.t.  $f_i(\mathbf{x}) < f_i(\mathbf{x}')$ . In general, there will not be a single dominating solution  $\mathbf{x}^*$ ; instead, we define the set of non-dominated solutions (i.e. the true *Pareto frontier*  $\mathcal{P}^*$ ),

$$\mathcal{P}^* := \{\mathbf{x} \in \mathcal{X} \mid \{\mathbf{x}' \in \mathcal{X} \mid \mathbf{x}' > \mathbf{x}, \mathbf{x}' \neq \mathbf{x}\} = \emptyset\}. \quad (1)$$

Since  $\mathcal{P}^*$  is unknown, we seek a set of candidate solutions  $\mathcal{P}$  that are close in objective space to those in  $\mathcal{P}^*$ . We find these solutions by maximizing the hypervolume bounded by the extremal points in  $\mathcal{P} \cup \{\mathbf{x}_{\text{ref}}\}$ , where  $\mathbf{x}_{\text{ref}}$  is some reference solution.

### 2.2. BayesOpt

We provide a brief review of BayesOpt. For a more complete introduction, see Brochu et al. (2010) and Frazier (2018). BayesOpt constructs a probabilistic *surrogate model*  $\hat{f} \in \mathcal{F}$  which is trained to emulate  $f$  from a dataset  $\mathcal{D} := \{(\mathbf{x}_1, \mathbf{y}_1), \dots, (\mathbf{x}_n, \mathbf{y}_n)\}$ , where  $\mathbf{y}_i$  are noisy observations of  $f(\mathbf{x}_i)$  (e.g.  $\mathbf{y}_i = f(\mathbf{x}_i) + \varepsilon_i$ ,  $\varepsilon_i \sim \mathcal{N}(0, I)$ ). The surrogate predictive distribution is used to define an *acquisition function*  $a : \mathcal{X} \times \mathcal{F} \rightarrow \mathbb{R}$ , which in turn defines an *inner*

---

#### Algorithm 1 The BayesOpt outer loop

---

**Inputs:** hypothesis space  $\mathcal{F}$ , acquisition  $a$ , dataset  $\mathcal{D}_0$ .  
**for**  $i = 0, \dots, i_{\text{max}} - 1$  **do**  
    Fit  $\hat{f} \in \mathcal{F}$  to  $\mathcal{D}_i$ .  
     $\mathbf{x}_i^* = \min_{\mathbf{x} \in \mathcal{X}} a(\mathbf{x}, \hat{f})$ .  $\leftarrow$  the inner loop  
    Observe  $\mathbf{y}_i \sim p(\cdot | \mathbf{x}_i^*)$ .  
     $\mathcal{D}_{i+1} = \mathcal{D}_i \cup (\mathbf{x}_i^*, \mathbf{y}_i)$ .  
     $\mathcal{P}_{i+1} = \text{nondominated}(\mathcal{D}_{i+1})$ .  
**end**  
**return**  $\mathcal{P}_{i_{\text{max}}}$

---

*loop* optimization problem to select new query point(s). The objective function is then queried at the selected points and the surrogate is retrained on the augmented dataset, and the procedure repeats, forming an *outer loop* (Algorithm 1).

Gaussian processes (GPs) (Williams & Rasmussen, 2006) are often preferred as surrogates due to their data efficiency, well-calibrated uncertainty estimates, and closed-form posterior distributions. The inductive biases of a GP are primarily determined by the choice of kernel, which defines a prior distribution over the values of  $f$  for any finite collection of inputs. Most commonly used GP kernels (e.g. RBF or Matérn) rely on  $\ell_2$  distance between inputs to determine the prior covariance between outputs. When the inputs are low-dimensional (e.g.  $d = 10$ ) such kernels work well, but in high dimensions the  $\ell_2$  norm is often a poor choice of distance metric (Srinivas et al., 2010; Wang et al., 2016). This limitation has motivated the development of *deep kernel learning* (DKL), which learns a low-dimensional continuous embedding via an encoder such as a convolutional neural network (CNN) (Wilson et al., 2016). Although GPs are kernel-based models, there is a range of well-known methods to scale them to large, online datasets, notably inducing point methods like stochastic variational GPs (SVGPs) which admit the use of stochastic optimizers (Hensman et al., 2013; Maddox et al., 2021c).

## 3. Related Work

**Discrete Optimization by Sampling.** Evolutionary algorithms such as NSGA-II (Deb et al., 2002), which slowly evolve a good solution by random mutation are a simple, popular baseline for BBO problems. However, NSGA-II is known for being sample inefficient (Turner et al., 2021). Discrete search methods that mutate specific residues incorporate expert knowledge about the protein family of interest, but cast the inner-loop optimization as a combinatorial problem, and rely on randomness to ensure batch diversity (Yang et al., 2019). Nigam et al. (2019) combine genetic algorithms and neural networks to optimize multi-objective chemical properties. The LaMBO architecture is inspired by “iterative resampling” approaches to sequence design

and machine translation (Gligorijevic et al., 2021; Lee et al., 2018; Zhang et al., 2021).

**Discrete BayesOpt.** Discrete BayesOpt methods can be categorized by how they structure the inner loop optimization problem. Some methods use substring kernels (SSKs) and genetic optimizers to work directly in sequence space (Lodhi et al., 2002; Beck & Cohn, 2017; Moss et al., 2020), but only consider small design tasks. Khan et al. (2022) is an example of concurrent work on antibody design in this vein, and copes with the inability of SSKs to scale to long sequences by only optimizing certain complementarity-determining regions (CDRs) of the antibody sequence. Latent-space optimizers learn continuous sequence embeddings, which are shared by a generative decoder modeling  $p(\mathbf{x})$  and the discriminative surrogate modeling  $p(\mathbf{y}|\mathbf{x})$  (Gómez-Bombarelli et al., 2018; Grosnit et al., 2021). The shared embeddings are optimized with gradient-based methods to produce new sequences. Deshwal & Doppa (2021) combined string kernels and deep VAE kernels, finding improved performance over simple latent space approaches in the very data-scarce regime ( $n \leq 100$ ).

At the time of writing, LaMBO is most similar to Latent-Space BayesOpt (LSBO) (Gómez-Bombarelli et al., 2018), since both methods train GP heads on top of latent representations decoded by a generative model and exploit the latent representation for inner loop optimization. LSBO uses a large pretraining dataset and a VAE with a specialized architecture (Jin et al., 2018) to solve a single-objective small-molecule design task, training the VAE and GP head separately. Because the GP cannot directly affect the embeddings, follow-up work by Tripp et al. (2020) proposed biasing the VAE objective towards high-scoring sequences in order to make the latent representations more useful to the GP. Aside from LaMBO’s use of DAEs rather than VAEs, this work substantially improves upon LSBO in multiple ways, such as enabling the use of general-purpose sequence model architectures, removing the pretraining requirement, providing a reliable procedure for jointly training generative and GP heads with a shared encoder, and the introduction of multi-objective acquisition functions. In concurrent work, Maus et al. (2022) combine a VAE-based architecture with trust-region BayesOpt for single-objective sequence design.

**Multi-Objective BayesOpt.** Daulton et al. (2020) proposed a batch version of the expected hypervolume improvement (EHVI) (Emmerich, 2005; Emmerich et al., 2011), an extension of the standard expected improvement (EI) acquisition (Jones et al., 1998) to multiple objectives. In follow-up work, Daulton et al. (2021a) proposed the noisy expected hypervolume improvement (NEHVI) acquisition function, which extends the noisy expected improvement (NEI) acquisition (Letham et al., 2019) to multiple objec-

tives. Multi-task GPs (MTGPs) have previously been used as surrogates for multi-objective BayesOpt (Shah & Ghahramani, 2016), including recent work scaling MTGPs up to thousands of training examples or objectives in the continuous setting (Daulton et al., 2021b; Maddox et al., 2021a). We make use of NEHVI and MTGPs, including an efficient MTGP posterior sampling approach developed in Maddox et al. (2021b).

## 4. Latent-Space Multi-Objective BayesOpt

We now describe the key ideas behind LaMBO, shown in Figure 2 and Algorithm 2.

### 4.1. Architecture Overview

We use a non-autoregressive denoising autoencoder to map discrete sequences to and from sequences of continuous token-level representations, with a multi-task GP head operating on pooled sequence-level representations. Unlike previous work combining GPs with deep generative models, our architecture does not require pretraining, nor do we require the surrogate to be completely reinitialized after receiving new data. Furthermore, we demonstrate that both stochastic variational and exact inference can be used, alleviating concerns regarding computational scalability or applicability to non-Gaussian objectives. Our models are implemented in BoTorch (Balandat et al., 2020), and GPyTorch (Gardner et al., 2018). See Appendix B for more implementation details.

**Shared Encoder.** We consider non-autoregressive bidirectional encoders  $g(\mathbf{x}, \theta_{\text{enc}}) = [\mathbf{z}_1, \dots, \mathbf{z}_t] = Z$ , where  $\mathbf{z}_i \in \mathbb{R}^d$  are latent token-level embeddings. In particular, our encoder is composed of 1D CNN layers, using standard vocabulary embeddings and sinusoidal position embeddings, padding token masking, skip-connections, and layernorm. A key advantage of using a DAE rather than a VAE is that projects like TAPE and ESM have already openly released large DAE models trained on massive protein corpora (Rives et al., 2021; Rao et al., 2019). As a result, encoders from these models could be used as drop-in replacements for the small CNN encoder we use.

**Discriminative Head.** This head takes an encoded sequence  $Z$  and outputs a scalar value indicating the utility of selecting that sequence as a query point. We pass  $Z$  to a discriminative encoder  $w$  to obtain transformed embeddings  $Z'$ , then pool  $Z'$  into low-dimensional sequence-level features. The discriminative encoder is smaller than the shared encoder, for example a single residual CNN block. The pooling operation  $(|\mathcal{I}(\mathbf{x})|)^{-1} \sum_{i \in \mathcal{I}(\mathbf{x})} \mathbf{z}'_i$  averages token-level embeddings over a restricted index set  $\mathcal{I}(\mathbf{x})$  which excludes positions corresponding to padding tokens. We define a

multi-task GP kernel by combining a 5/2 Matérn kernel evaluated on these sequence features with an intrinsic model of coregionalization (ICM) kernel over  $f_i$  (Goovaerts et al., 1997; Alvarez et al., 2011; Rasmussen & Williams, 2008). The resulting GP outputs a posterior predictive distribution  $p(f|\mathcal{D})$ , which is passed as input to the acquisition function. We use the noisy expected hypervolume improvement (NEHVI) acquisition from Daulton et al. (2021a) since some objectives (particularly those involving biological data) are inherently noisy.

**Decoder Head.** The generative decoder head  $h$  maps a sequence of token-level embeddings to a predictive distribution over  $\mathcal{X}$  and can either be a simple masked language model (MLM) head (Devlin et al., 2018) or a full seq2seq latent non-autoregressive neural machine translation (LANMT) decoder (Shu et al., 2020). In this work we make use of both. An MLM head is simpler and easier to control than an LANMT decoder, which allows for careful comparisons between LaMBO and discrete genetic optimizers. Despite their complexity, LANMT decoders accommodate insertions and deletions more gracefully than MLM heads by means of a length prediction head and length transform operation, allowing the same latent representation to be decoded to sequences of varying length. In either case, the decoder uses the same layer types as the shared encoder  $g$ , and takes both  $Z$  and  $Z'$  as input.

## 4.2. Initializing the Latent Embeddings

At each outer-loop iteration  $i$ , there are many choices of  $\mathbf{x}$  we are confident will *not* improve our current solution  $\mathcal{P}_i$ , resulting in large flat regions of the inner-loop loss surface when using acquisition functions like EI and NEHVI. If the inner-loop is not initialized carefully, it is very likely the initial solution will fall in one of these flat regions, severely hampering gradient-based optimization. If  $\mathbf{x}$  was continuous, we could use initialization heuristics from previous work to avoid this pitfall (Balandat et al., 2020; Daulton et al., 2021a). Instead we now show how the the same corruption process used to train and sample from DAEs can be used as a robust initialization procedure for discrete  $\mathbf{x}$  by initializing the inner loop solution in latent-space ( $Z_0$ ) with corrupted, encoded variants of the current outer-loop solution  $\mathcal{P}_i$ .

**Selecting base sequences.** We begin with a set of seed sequences  $\mathcal{X}_{\text{pool}}$  and select a subset,  $\mathcal{X}_{\text{base}} \subset \mathcal{X}_{\text{pool}}$ . After each optimization round, the latest query sequences are added to  $\mathcal{X}_{\text{pool}}$  and can serve as future base sequences. Choosing  $\mathcal{X}_{\text{base}}$  well is critical for fast convergence. If too many low quality sequences are added, too much computation is spent optimizing them. Conversely, only selecting the current Pareto sequences could hinder exploration of

**Algorithm 2** The LaMBO inner loop. For clarity, steps where LaMBO differs from LSBO are shown in blue.

**Inputs:** acquisition  $a$ , corruption  $c$ , shared encoder  $g$ , discriminative encoder  $w$ , decoder  $h$ , base sequences  $\mathcal{X}_{\text{base}}$ , and batch size  $b$ .

```

 $v^* \leftarrow +\infty$ 
 $Z_0 = \{g \circ c(\mathbf{x}_0), \dots, g \circ c(\mathbf{x}_b)\}, \mathbf{x}_m \in \mathcal{X}_{\text{base}}$ 
for  $j = 0, \dots, j_{\text{max}}$  do
     $Z'_j = w(Z_j)$ 
     $Z_{j+1} = Z_j - \eta \nabla_Z [a(Z'_j) - \lambda \mathbb{H}[h(Z_j, Z'_j)]]$ 
     $\mathcal{X}_{\text{cand}} \leftarrow \{\mathbf{x}'_1, \dots, \mathbf{x}'_b\} \sim h(Z_j, Z'_j)$ 
     $Z_{\text{cand}} \leftarrow [g(\mathbf{x}'_1), \dots, g(\mathbf{x}'_b)]^\top$ 
     $v_j = a(w(Z_{\text{cand}}))$ 
    if  $v_j < v^*$  then
         $v^*, \mathcal{X}^* \leftarrow v_j, \mathcal{X}_{\text{cand}}$ 
    end
end
return  $\mathcal{X}^*$ 
    
```

sequences with potential for improvement. The interaction between the online queries and the decoder head must also be considered, since we want to prevent the generative samples from collapsing to a couple sequences.

We populate  $\mathcal{X}_{\text{base}}$  first with the current Pareto sequences  $\mathcal{P}_i$ , then with random sequences (without replacement) that were on the Pareto frontier in previous optimization rounds ( $\mathcal{P}_{<i}$ ), and finally fill any remaining space in the base set with random sequences from the entire optimization history. In practice, we took the size of the base set to be the same as the query batch size  $b$ . We perform multiple restarts during the inner loop, and each restart samples  $b$  sequences from  $\mathcal{X}_{\text{base}}$ , with replacement.

We do not sample any base sequences uniformly at random, but according to a weighted distribution  $\Delta(\mathcal{X}_{\text{pool}})$  to ensure that high-scoring sequences are more likely to be optimized than low-scoring ones. Let  $r_i(\mathbf{x}_j, X)$  be the rank of  $\mathbf{x}_j \in X$  w.r.t. the 0-indexed dense ranking of  $X$  according to  $f_i$ , and let  $r_{\max}(\mathbf{x}_j, X) = \max_{\mathbf{x}_i} r_i(\mathbf{x}_j, X)$ . The sampling weight  $w_j$  of  $\mathbf{x}_j \in \mathcal{X}_{\text{pool}}$  is

$$w_j = s_j(-\log(1 + \mathbf{r})/\tau), \quad (2)$$

$$\mathbf{r} = [r_{\max}(\mathbf{x}_1, X), \dots, r_{\max}(\mathbf{x}_p, X)],$$

where  $s_j(\mathbf{v}) = \exp(v_j) / \sum_i \exp(v_i)$  is the softmax function and  $\tau \in (0, +\infty)$  is the softmax temperature. In other words, we choose the least favorable ranking across all objectives for each  $\mathbf{x}$  to determine its weight. This type of weighting is similar in spirit to a procedure used by Tripp et al. (2020) to bias the training objective of generative models in favor of high-scoring sequences.

**Selecting base sequence positions.** After obtaining  $\mathcal{X}_{\text{base}}$  we apply a corruption function  $c$  to each element

before passing them as input to the encoder, similar to the procedure proposed in [Gligorijevic et al. \(2021\)](#). The corruption function first selects positions in each sequence to modify, then selects a modification (substitution, insertion, deletion) at those positions. We uniformly sample positions not occupied by special tokens, such as padding tokens.

**Selecting corruption operations.** Once sequence positions have been selected, the corruption function chooses corruption operations to apply at those positions. For LaMBO, the corruption procedure differs depending on whether the decoder is an MLM head or a LANMT head. If the decoder is an MLM head then all operations are substitution operations, and the replacement tokens are all masking tokens. If the decoder is an LANMT head then the operation type is chosen randomly and replacement tokens are sampled uniformly from  $\mathcal{V}$ . Note we use a similar corruption procedure to train the decoder head.

### 4.3. Sequence Optimization

At a high level, we solve the inner-loop by treating the output of the decoder head  $h$  as a proposal distribution. We iteratively refine the proposal distribution by following a regularized acquisition gradient in latent space, drawing and scoring batches of sequences along the way (Algorithm 2).

More precisely, once we have selected and corrupted the base sequences, we pass them through the encoder to produce latent embeddings  $Z_0$  that serve as the initial solution for the inner-loop optimization problem. Then for each optimization step  $0 \leq i < i_{\max}$ , we take  $Z_{j+1} = Z_j - \eta \nabla_Z [\ell_{\text{query}}(Z_j)]$ , where  $Z'_j = w(Z_j)$  (i.e. the output of the discriminative encoder  $w$ ),

$$\ell_{\text{query}}(Z_j) = a(Z'_j) + \lambda \mathbb{H}[h(Z_j, Z'_j)], \quad (3)$$

$\mathbb{H}$  is the Shannon entropy, and  $\eta$ ,  $\lambda$  are hyperparameters controlling the step-size and regularization strength. We sample  $\mathcal{X}_{\text{batch}} = \{\mathbf{x}'_0, \dots, \mathbf{x}'_b\} \sim h(Z_j, Z'_j)$ , and score  $\mathcal{X}_{\text{batch}}$  by passing it *uncorrupted* through the shared encoder and discriminative head. If we see that  $\mathcal{X}_{\text{batch}}$  has the best acquisition value so far, we store it and continue optimizing. Note that this procedure produces a different result than simply optimizing  $Z$  and decoding once at the end. Recall that the decoder is stochastic, and the ultimate goal of the inner loop is to produce *sequences* with high acquisition value, not just sequences sampled from high-scoring latent embeddings.

We observed that following the unregularized acquisition gradient caused the decoder entropy to quickly increase, resulting in very uniform proposal distributions. When the proposal distributions are uniform, LaMBO essentially performs a variant of random search. However, because  $Z_0$  is produced in the same way the decoder head is trained (i.e.

the same corruption process), we expect that it will be close to other latent embeddings seen during training, and the decoder entropy will be relatively low. These observations motivated us to include the proposal entropy penalty in Eq. (3), to encourage  $Z_j$  to stay in a region of latent space where the decoder has non-uniform predictive distributions.

We also considered choosing a small step-size  $\eta$  to implicitly confine  $Z_j$  to a small region around  $Z_0$ , but we found it difficult to choose  $\eta$  both large enough to improve the acquisition value and small enough to prevent uniform proposals. The proposal entropy penalty also has the added benefit of smoothing the query loss surface when using acquisitions like NEHVI, which helps make the inner loop less dependent on a good initialization. Adding a regularization term for improved control of the acquisition function has been previously studied in the continuous setting by [Shahriari et al. \(2016\)](#).

## 5. Experimental Evaluation

We now apply LaMBO to a series of increasingly difficult small-molecule and large-molecule sequence design tasks. We first describe the suite of tasks, including a new multi-objective large-molecule task which involves jointly maximizing the solvent-accessible surface area (SASA) and the stability of RFPs. We then demonstrate that LaMBO outperforms strong genetic baselines in a carefully controlled comparison, followed by a series of investigative experiments to give insight into the design choices behind LaMBO. Finally we show that LaMBO compares favorably with LSBO (a well-known single-objective discrete BayesOpt algorithm). Our findings show that with only a couple hundred initial labels LaMBO can successfully optimize sequences with hundreds of tokens for multiple objectives.

### 5.1. Evaluation procedure

We consider the following *in silico* multi-objective evaluation tasks:

- **Bigrams:** optimize short strings (around 32 tokens) uniformly sampled from  $\mathcal{X}$  to maximize the counts of multiple bigrams (Appendix A.1).
- **ZINC:** optimize SELFIES-encoded small molecules (usually 50-100 tokens) from the ZINC dataset to maximize logP and QED (Appendix A.2).
- **FP:** optimize red-spectrum fluorescent protein sequences (around 200 tokens) from the FPBase dataset to maximize stability and SASA (Appendix A.3).

The appendix contains full details of each task. Note that the **RFP** task is a novel contribution in this work, requiring the program to optimize objectives computed from the 3D

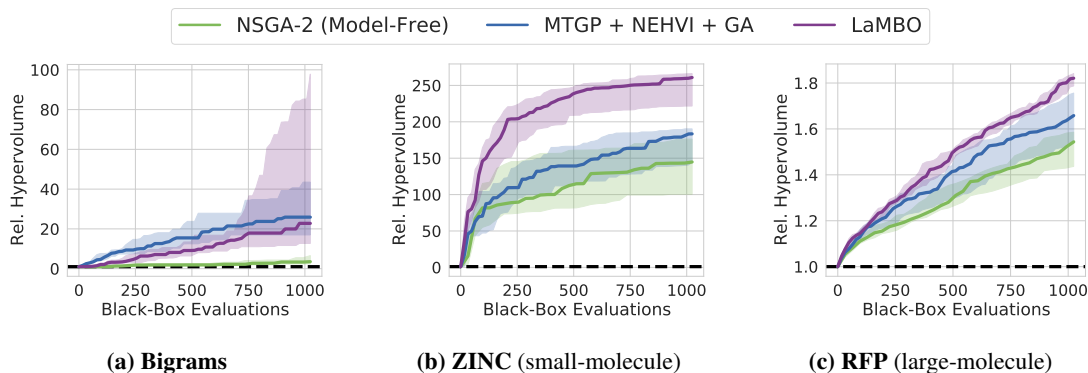


Figure 3. On all three tasks (described in Section 5.1), LaMBO outperforms genetic algorithm baselines, specifically NSGA-2 and a model-based genetic optimizer with the same surrogate architecture (MTGP + NEHVI + GA). Performance is quantified by the hypervolume bounded by the optimized Pareto frontier. The midpoint, lower, and upper bounds of each curve depict the 50%, 20%, and 80% quantiles, estimated from 10 trials. See Section 5.2 for more discussion.

protein structure given only residue sequences and a high-latency simulation oracle.

Unless otherwise noted, each task begins with 512 examples in its start pool, and collects a total of 1024 online queries in batches of 16. No additional pretraining data is used. Each method uses the same architecture and hyperparameters for all tasks. The methods are evaluated by comparing the hypervolume bounded by the Pareto front after  $x$  black-box function calls, relative to the starting hypervolume. Relative hypervolume greater than 1 indicates improvement.

## 5.2. Comparing to Multi-Objective Genetic Optimizers

In Figure 3 we compare LaMBO with a MLM decoder head against two genetic algorithm (GA) baselines. For this experiment we set the entropy penalty at  $\lambda = 0.01$ . The simplest baseline is NSGA-2, a robust model-free multi-objective genetic optimization routine. The other baseline is a model-

based GA which screens query sequences with the same surrogate and acquisition function (NEHVI) as LaMBO. Both GA baselines use a uniform proposal distribution.

In this experiment all optimizers are only allowed to change a single token per optimization round, and each optimizer selects base sequences and token positions in the same way. In fact LaMBO can be viewed as a generalization of the model-based GA, where the replacement token distribution is learned and optimized, rather than fixed *a priori*. Notably, the model-based GA differs from LaMBO primarily in two respects: (1) the encoder is trained only through the supervised loss, and (2) replacement tokens are sampled uniformly. The effect of (2) is most strongly seen in **ZINC**, since the SELFIES vocabulary derived from the molecules in the ZINC dataset is significantly larger than the amino acid vocabulary used for proteins.

LaMBO performs well on all three tasks, particularly **ZINC** and **RFP**. In contrast to the natural sequences in molecular datasets, the starting distribution over sequences in **Bigrams** has the highest possible entropy, so LaMBO learns a good sampling distribution more slowly.

## 5.3. Analyzing LaMBO

Having demonstrated that LaMBO compares favorably to genetic optimizers, we now examine the different components of LaMBO and how each contributes to performance. In Figure 4, we evaluate the sensitivity of LaMBO to the choice of acquisition on the **RFP** task. We compare the final Pareto frontier obtained with a simple multi-objective scalarization (averaging normalized scores) to the frontier obtained with NEHVI. Score averaging focuses optimization on solutions with similar tradeoffs, pushing the interior of the frontier out quickly. This behavior leads to less exploration than NEHVI and thus a slightly lower hypervolume

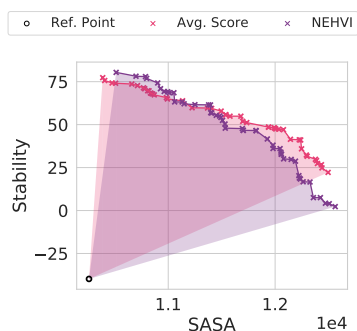


Figure 4. Pareto fronts of LaMBO and a variant that optimizes the expected average objective value on the **RFP** task. NEHVI incentivizes more exploration of the frontier extremities, resulting in solutions representing more diverse tradeoffs and slightly higher hypervolume.

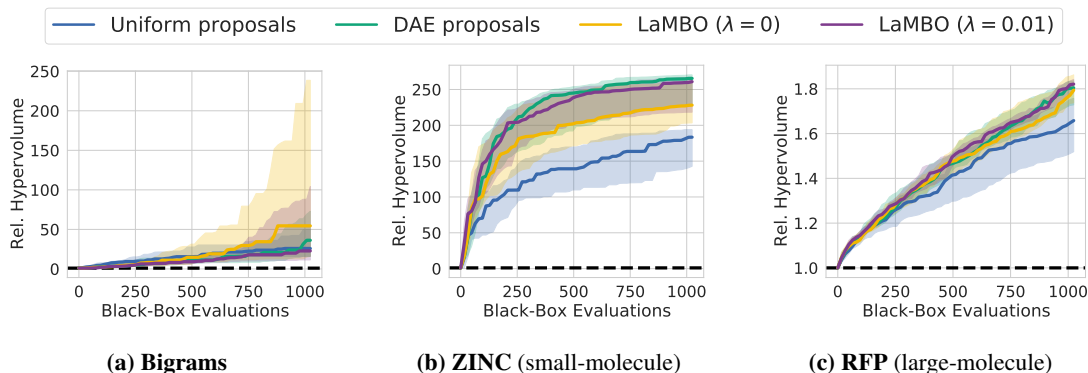


Figure 5. An ablation of LaMBO’s main components. Starting from our model-based GA baseline (uniform proposals), we cumulatively add the elements described in Section 4.3: (1) DAE-generated proposals, (2) DAE proposal optimization following  $\nabla_Z[\ell_{\text{query}}]$  with  $\lambda = 0$ . (see Eq. (3)), and (3) DAE proposal optimization with  $\lambda = 0.01$ . DAE proposals improve performance on all tasks. Proposal optimization is most helpful on **Bigrams** where the starting sequence distribution is very unlikely to produce high-scoring queries. Similarly the entropy penalty is useful when starting with a low-entropy, task-specific dataset of natural sequences (i.e. **ZINC** and **RFP**). The midpoint, lower, and upper bounds of each curve depict the 50%, 20%, and 80% quantiles, estimated from 10 trials.

of 1.51 as compared to NEHVI’s hypervolume of 1.57. Our findings corroborate similar results in previous work comparing scalarization and hypervolume-based acquisitions in different problem settings (Emmerich, 2005; Emmerich et al., 2011; Daulton et al., 2020).

In our next experiment we disentangle the effect of replacing a uniform proposal distribution with a DAE-generated one, and the effect of optimizing the DAE proposal distribution by gradient descent on  $\ell_{\text{query}}$ . In Figure 5 we interpolate between the model-based GA baseline in Figure 3 and LaMBO by cumulatively adding DAE-generated proposals, DAE proposal optimization, and the DAE entropy penalty. We find that unoptimized DAE proposals with NEHVI screening is a strong baseline on all tasks. DAE proposal optimization is the most useful in **Bigrams**, where the true non-dominated solutions  $\mathcal{P}^*$  lie far outside the starting sequence distribu-

tion, requiring more exploration. See Figure 8 in Appendix C for more discussion.

#### 5.4. What About Substring Kernels?

Since the start pools used in the evaluation in Figure 3 are fairly small (i.e. hundreds of examples), it is natural to wonder how a substring kernel (SSK) GP (e.g., Moss et al., 2020) would compete with our deep kernel learning (DKL) based GPs. Due to constraints on time and computation, and scalability challenges for the SSK, we do not directly compare SSK GPs and DKL GPs in the online setting. However, in Figure 6, we compare SSK GPs and DKL GPs in the offline regression setting, training both models only through the supervised loss to predict the SASA property of RFP large molecules, using 410 examples for training and 102 examples for validation and test. The SSK GP performs well, but is very under-confident when compared to the DKL GP.

SSKs have drawbacks at several levels. At a conceptual level, SSKs cannot identify regions of the sequence that have little effect on the objective values, since matching substrings increase the predictive covariance between sequences regardless of where the substrings are found. At a practical level, SSKs are difficult to integrate with deep generative models since they do not operate on continuous representations, and standard methods for scaling Gaussian processes — inducing point methods (e.g., Hensman et al., 2013), random feature expansions (e.g., Lázaro-Gredilla et al., 2010), and CG-based methods (e.g., Gardner et al., 2018) — are not naturally applicable (more discussion in Appendix B.4). At an empirical level, our experiments do not support the idea that SSK GPs are superior models for biological sequences. As a result it is hard to justify additional investment into SSK GPs for protein design.

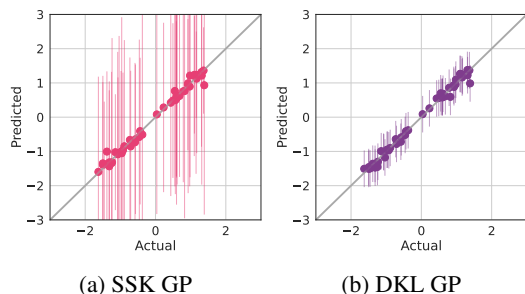


Figure 6. Evaluating the effect of kernel choice on exact GP regression with a discrete SSK (left) and a deep Matérn kernel with a CNN encoder (right) when predicting the SASA property of RFP large molecules. The SSK GP is under-confident and less accurate than the DKL GP, suggesting SSK GPs would not improve optimization performance.



### 5.5. Comparison to the single-objective LSBO

We now evaluate LaMBO in the single-objective setting, using the *penalized logP* task described in Tripp et al. (2020). In contrast to SSK-based methods, LaMBO can successfully be scaled to large datasets with standard variational GP inference, allowing us to compare to the popular latent space BayesOpt approach (LSBO) (Gómez-Bombarelli et al., 2018) on a larger-scale problem. The start pool for this task is composed of the 2000 highest scoring sequences from ZINC, and 8000 random sequences, replicating the setup in Tripp et al. (2020). To accommodate the larger dataset, the discriminative head uses  $k$  independent SVGPs with 64 shared inducing points rather than an exact MTGP.

In Figure 7 we demonstrate that LaMBO is competitive with a variant of LSBO specifically designed for this task, requiring about twice as many online observations before reaching the reported median best score attained by LSBO (Tripp et al., 2020). As noted in Section 3, LSBO uses the entire ZINC dataset for pretraining, so we do not directly compare sample efficiency. In addition to the differences between LaMBO and LSBO already noted, we use SELFIES encodings rather than SMILES. We use a seq2seq LANMT-style decoder head for this task, since the objective heavily favors large molecules. High-scoring molecules such as those found by LSBO are larger than any found in ZINC, so it is important that the optimizer allow insertions.

Overall, LaMBO outperforms the best reported LSBO score (27.84) by a wide margin, reaching scores as high as 50 for some seeds, while using a more general architecture and requiring less data (i.e. counting both pretraining data and online queries). The factor that ultimately bounds the penalized logP objective in practice is the max sequence length constraint imposed by the positional encoding scheme we use. Therefore we note that, despite its widespread use, unconstrained logP (penalized or otherwise) is a poor optimization benchmark, since it can be manipulated by altering the positional encoding to permit longer sequences (Nigam et al., 2019; Tripp et al., 2021; Fu et al., 2020).

In short, while LaMBO is designed to facilitate multi-objective optimization — a central feature of biological sequence design — it can also outperform the widely used single-objective LSBO, even in a single-objective setting.

## 6. Discussion

Biological sequence design is quickly becoming known as one of the most promising applications of machine learning. BayesOpt has extraordinary potential for this domain, but conventional approaches face several challenges associated with the high-dimensional, discrete, multi-objective setting. We have shown how deep generative models can be naturally integrated with BayesOpt to address these chal-

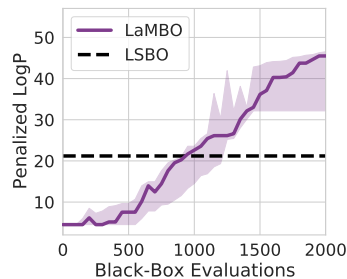


Figure 7. LaMBO reaches a higher objective value than the best reported LSBO result. When constrained to 500 evaluations LSBO is more sample efficient (ignoring pretraining data). The midpoint, lower, and upper bounds of the LaMBO curve depict the 60%, 40%, and 80% quantiles, estimated from 5 trials.

lenges, achieving sample efficiency and solution diversity across a range of sequence design tasks. Moreover, we introduced a new large-molecule benchmark, which provides a challenging and realistic setting for protein design. In this benchmark, we must optimize multiple objectives computed from 3D protein structure given only residue sequences and a high-latency simulation oracle.

In the short term, it will be exciting to investigate whether large pre-trained encoders can be combined with specialized sequence modeling techniques (Rao et al., 2019; Rives et al., 2021; Ruffolo et al., 2021) for protein design. The initialization procedure in Section 4.2 could also be improved by prioritizing mutation locations that are likely to affect the objective values. In the longer run, there are also many promising developments in BayesOpt methodology that are yet to be explored for sequence design, such as non-myopic acquisition functions (Jiang et al., 2020), multi-fidelity acquisition functions to determine the type of experimental assay and number of replications (Kandasamy et al., 2017; Wu et al., 2019), rigorous treatment of optimization constraints (Eriksson et al., 2019), and the coordination of many parallel drug development campaigns by optimizing risk measures across a whole compound portfolio (Cakmak et al., 2020). BayesOpt with multi-modal inputs is a particularly exciting direction, allowing scientists to combine many different sources of experimental data, including 3D structure and raw instrumental output (Jin et al., 2021). BayesOpt itself can also be developed for better adaptivity to misspecification, miscalibration, and distribution shift, all of which are important in drug design problems. Finally, our work also highlights the need for good benchmarks to evaluate methods in sequence design.

While there are still many challenges to overcome, there is a path for Bayesian optimization to revolutionize drug design, profoundly improving our lives, and changing the way we approach scientific discovery.

**Acknowledgements.** We would like to thank Andres Potapczynski and Sanyam Kapoor for helpful discussions. This research is supported by an Amazon Research Award, Facebook Research, Google Research, NSF I-DISRE 193471, NIH R01DA048764-01A1, NSF IIS-1910266, and NSF 1922658 NRT-HDR.

## References

- Alvarez, M. A., Rosasco, L., and Lawrence, N. D. Kernels for vector-valued functions: A review. *arXiv preprint arXiv:1106.6251*, 2011.
- Angermueller, C., Belanger, D., Gane, A., Mariet, Z., Dohan, D., Murphy, K., Colwell, L., and Sculley, D. Population-based black-box optimization for biological sequence design. In *International Conference on Machine Learning*, pp. 324–334. PMLR, 2020.
- Baek, M., DiMaio, F., Anishchenko, I., Dauparas, J., Ovchinnikov, S., Lee, G. R., Wang, J., Cong, Q., Kinch, L. N., Schaeffer, R. D., et al. Accurate prediction of protein structures and interactions using a three-track neural network. *Science*, 373(6557):871–876, 2021.
- Balandat, M., Karrer, B., Jiang, D., Daulton, S., Letham, B., Wilson, A. G., and Bakshy, E. BoTorch: A Framework for Efficient Monte-Carlo Bayesian Optimization. In *Advances in Neural Information Processing Systems*, volume 33, 2020. URL <https://proceedings.neurips.cc/paper/2020/hash/f5b1b89d98b7286673128a5fb112cb9a-Abstract.html>.
- Beck, D. and Cohn, T. Learning kernels over strings using gaussian processes. In *Proceedings of the Eighth International Joint Conference on Natural Language Processing (Volume 2: Short Papers)*, pp. 67–73, 2017.
- Bickerton, G. R., Paolini, G. V., Besnard, J., Muresan, S., and Hopkins, A. L. Quantifying the chemical beauty of drugs. *Nature chemistry*, 4(2):90–98, 2012.
- Biswas, S., Khimulya, G., Alley, E. C., Esvelt, K. M., and Church, G. M. Low-n protein engineering with data-efficient deep learning. *Nature Methods*, 18(4):389–396, 2021.
- Blank, J. and Deb, K. Pymoo: Multi-objective optimization in python. *IEEE Access*, 8:89497–89509, 2020.
- Brochu, E., Cora, V. M., and De Freitas, N. A tutorial on bayesian optimization of expensive cost functions, with application to active user modeling and hierarchical reinforcement learning. *arXiv preprint arXiv:1012.2599*, 2010.
- Cakmak, S., Astudillo Marban, R., Frazier, P., and Zhou, E. Bayesian optimization of risk measures. *Advances in Neural Information Processing Systems*, 33:20130–20141, 2020.
- Chudakov, D. M., Matz, M. V., Lukyanov, S., and Lukyanov, K. A. Fluorescent proteins and their applications in imaging living cells and tissues. *Physiological Reviews*, 90(3):1103–1163, 2010. doi: 10.1152/physrev.00038.2009. URL <https://doi.org/10.1152/physrev.00038.2009>. PMID: 20664080.
- Cock, P. J., Antao, T., Chang, J. T., Chapman, B. A., Cox, C. J., Dalke, A., Friedberg, I., Hamelryck, T., Kauff, F., Wilczynski, B., et al. Biopython: freely available python tools for computational molecular biology and bioinformatics. *Bioinformatics*, 25(11):1422–1423, 2009.
- Dance, A. The hunt for red fluorescent proteins. *Nature*, 596:152–153, August 2021. (Online) <https://doi.org/10.1038/d41586-021-02093-6>.
- Daulton, S., Balandat, M., and Bakshy, E. Differentiable Expected Hypervolume Improvement for Parallel Multi-Objective Bayesian Optimization. *Advances in Neural Information Processing Systems*, 33, 2020. URL <https://proceedings.neurips.cc/paper/2020/hash/6fec24eac8f18ed793f5eaad3dd7977c-Abstract.html>.
- Daulton, S., Balandat, M., and Bakshy, E. Parallel bayesian optimization of multiple noisy objectives with expected hypervolume improvement. *arXiv preprint arXiv:2105.08195*, 2021a.
- Daulton, S., Eriksson, D., Balandat, M., and Bakshy, E. Multi-objective bayesian optimization over high-dimensional search spaces. *arXiv preprint arXiv:2109.10964*, 2021b.
- Deb, K., Pratap, A., Agarwal, S., and Meyarivan, T. A fast and elitist multiobjective genetic algorithm: Nsga-ii. *IEEE transactions on evolutionary computation*, 6(2): 182–197, 2002.
- Deshwal, A. and Doppa, J. Combining latent space and structured kernels for bayesian optimization over combinatorial spaces. *Advances in Neural Information Processing Systems*, 34, 2021.
- Devlin, J., Chang, M.-W., Lee, K., and Toutanova, K. Bert: Pre-training of deep bidirectional transformers for language understanding. *arXiv preprint arXiv:1810.04805*, 2018.
- Emmerich, M. Single-and multi-objective evolutionary design optimization assisted by gaussian random field meta-models. *dissertation, Universität Dortmund*, 2005.

- Emmerich, M. T., Deutz, A. H., and Klinkenberg, J. W. Hypervolume-based expected improvement: Monotonicity properties and exact computation. In *2011 IEEE Congress of Evolutionary Computation (CEC)*, pp. 2147–2154. IEEE, 2011. URL <https://www.biorxiv.org/content/early/2021/06/28/2021.06.26.450037>.
- Jiang, S., Jiang, D., Balandat, M., Karrer, B., Gardner, J., and Garnett, R. Efficient nonmyopic bayesian optimization via one-shot multi-step trees. *Advances in Neural Information Processing Systems*, 33:18039–18049, 2020.
- Jin, W., Barzilay, R., and Jaakkola, T. Junction tree variational autoencoder for molecular graph generation. In *International conference on machine learning*, pp. 2323–2332. PMLR, 2018.
- Jin, W., Wohlwend, J., Barzilay, R., and Jaakkola, T. Iterative refinement graph neural network for antibody sequence-structure co-design. *arXiv preprint arXiv:2110.04624*, 2021.
- Jones, D. R., Schonlau, M., and Welch, W. J. Efficient global optimization of expensive black-box functions. *Journal of Global optimization*, 13(4):455–492, 1998.
- Jumper, J., Evans, R., Pritzel, A., Green, T., Figurnov, M., Ronneberger, O., Tunyasuvunakool, K., Bates, R., Žídek, A., Potapenko, A., et al. Highly accurate protein structure prediction with alphafold. *Nature*, 596(7873):583–589, 2021.
- Kandasamy, K., Dasarathy, G., Schneider, J., and Póczos, B. Multi-fidelity bayesian optimisation with continuous approximations. In *International Conference on Machine Learning*, pp. 1799–1808. PMLR, 2017.
- Khan, A., Cowen-Rivers, A. I., Deik, D.-G.-X., Grosnit, A., Dreckowski, K., Robert, P. A., Greiff, V., Tutunov, R., Bou-Ammar, D., Wang, J., et al. Antbo: Towards real-world automated antibody design with combinatorial bayesian optimisation. *arXiv preprint arXiv:2201.12570*, 2022.
- Krenn, M., Häse, F., Nigam, A., Friederich, P., and Aspuru-Guzik, A. Self-referencing embedded strings (selfies): A 100% robust molecular string representation. *Machine Learning: Science and Technology*, 1(4):045024, 2020.
- Lambert, T. J. Fpbase: a community-editable fluorescent protein database. *Nature methods*, 16(4):277–278, 2019.
- Lázaro-Gredilla, M., Quinero-Candela, J., Rasmussen, C. E., and Figueiras-Vidal, A. R. Sparse spectrum gaussian process regression. *The Journal of Machine Learning Research*, 2010.
- Lee, J., Mansimov, E., and Cho, K. Deterministic non-autoregressive neural sequence modeling by iterative refinement. *arXiv preprint arXiv:1802.06901*, 2018.
- Emmerich, M. T., Deutz, A. H., and Klinkenberg, J. W. Hypervolume-based expected improvement: Monotonicity properties and exact computation. In *2011 IEEE Congress of Evolutionary Computation (CEC)*, pp. 2147–2154. IEEE, 2011.
- Eriksson, D., Pearce, M., Gardner, J., Turner, R. D., and Poloczek, M. Scalable global optimization via local bayesian optimization. *Advances in Neural Information Processing Systems*, 32:5496–5507, 2019.
- Ertl, P. and Schuffenhauer, A. Estimation of synthetic accessibility score of drug-like molecules based on molecular complexity and fragment contributions. *Journal of cheminformatics*, 1(1):1–11, 2009.
- Frazier, P. I. A tutorial on bayesian optimization. *arXiv preprint arXiv:1807.02811*, 2018.
- Fu, T., Xiao, C., Li, X., Glass, L. M., and Sun, J. Mimoso: Multi-constraint molecule sampling for molecule optimization. *arXiv preprint arXiv:2010.02318*, 2020.
- Gardner, J., Pleiss, G., Weinberger, K. Q., Bindel, D., and Wilson, A. G. Gpytorch: Blackbox matrix-matrix gaussian process inference with gpu acceleration. *Advances in Neural Information Processing Systems*, 31:7576–7586, 2018.
- Gligorijevic, V., Berenberg, D., Ra, S., Watkins, A., Kelow, S., Cho, K., and Bonneau, R. Function-guided protein design by deep manifold sampling. *bioRxiv*, 2021.
- Gómez-Bombarelli, R., Wei, J. N., Duvenaud, D., Hernández-Lobato, J. M., Sánchez-Lengeling, B., Sheberla, D., Aguilera-Iparraguirre, J., Hirzel, T. D., Adams, R. P., and Aspuru-Guzik, A. Automatic chemical design using a data-driven continuous representation of molecules. *ACS central science*, 4(2):268–276, 2018.
- Goovaerts, P. et al. *Geostatistics for natural resources evaluation*. Oxford University Press on Demand, 1997.
- Grosnit, A., Tutunov, R., Maraval, A. M., Griffiths, R.-R., Cowen-Rivers, A. I., Yang, L., Zhu, L., Lyu, W., Chen, Z., Wang, J., et al. High-dimensional bayesian optimisation with variational autoencoders and deep metric learning. *arXiv preprint arXiv:2106.03609*, 2021.
- Hensman, J., Fusi, N., and Lawrence, N. D. Gaussian processes for big data. *arXiv preprint arXiv:1309.6835*, 2013.
- Høie, M. H., Cagiada, M., Frederiksen, A. H. B., Stein, A., and Lindorff-Larsen, K. Predicting and interpreting large scale mutagenesis data using analyses of protein stability and conservation. *bioRxiv*, 2021. doi: 10.1101/2021.06.26.450037.

- Letham, B., Karrer, B., Ottoni, G., and Bakshy, E. Constrained bayesian optimization with noisy experiments. *Bayesian Analysis*, 14(2):495–519, 2019.
- Lipinski, C. A., Lombardo, F., Dominy, B. W., and Feeney, P. J. Experimental and computational approaches to estimate solubility and permeability in drug discovery and development settings. *Advanced drug delivery reviews*, 23(1-3):3–25, 1997.
- Lodhi, H., Saunders, C., Shawe-Taylor, J., Cristianini, N., and Watkins, C. Text classification using string kernels. *Journal of Machine Learning Research*, 2(Feb):419–444, 2002.
- Maddox, W., Feng, Q., and Balandat, M. Optimizing high-dimensional physics simulations via composite bayesian optimization. *arXiv preprint arXiv:2111.14911*, 2021a.
- Maddox, W. J., Balandat, M., Wilson, A. G., and Bakshy, E. Bayesian optimization with high-dimensional outputs. *Advances in Neural Information Processing Systems*, 34, 2021b.
- Maddox, W. J., Stanton, S., and Wilson, A. G. Conditioning sparse variational gaussian processes for online decision-making. *Advances in Neural Information Processing Systems*, 34, 2021c.
- Maus, N., Jones, H. T., Moore, J. S., Kusner, M. J., Bradshaw, J., and Gardner, J. R. Local latent space bayesian optimization over structured inputs. *arXiv preprint arXiv:2201.11872*, 2022.
- Meier, J., Rao, R., Verkuil, R., Liu, J., Sercu, T., and Rives, A. Language models enable zero-shot prediction of the effects of mutations on protein function. *bioRxiv*, 2021.
- Mishra, A., Ranganathan, S., Jayaram, B., and Sattar, A. Role of solvent accessibility for aggregation-prone patches in protein folding. *Scientific Reports*, 8(1):12896, 2018. doi: 10.1038/s41598-018-31289-6. URL <https://doi.org/10.1038/s41598-018-31289-6>.
- Moss, H. B., Beck, D., Gonzalez, J., Leslie, D. S., and Rayson, P. Boss: Bayesian optimization over string spaces. *arXiv preprint arXiv:2010.00979*, 2020.
- Nigam, A., Friederich, P., Krenn, M., and Aspuru-Guzik, A. Augmenting genetic algorithms with deep neural networks for exploring the chemical space. *arXiv preprint arXiv:1909.11655*, 2019.
- O’Donoghue, B., Osband, I., Munos, R., and Mnih, V. The uncertainty bellman equation and exploration. In *International Conference on Machine Learning*, pp. 3836–3845, 2018.
- Paszke, A., Gross, S., Massa, F., Lerer, A., Bradbury, J., Chanan, G., Killeen, T., Lin, Z., Gimelshein, N., Antiga, L., et al. Pytorch: An imperative style, high-performance deep learning library. *Advances in neural information processing systems*, 32:8026–8037, 2019.
- Rao, R., Bhattacharya, N., Thomas, N., Duan, Y., Chen, X., Canny, J., Abbeel, P., and Song, Y. S. Evaluating protein transfer learning with tape. *Advances in neural information processing systems*, 32:9689, 2019.
- Rasmussen, C. E. and Williams, C. K. I. *Gaussian processes for machine learning*. Adaptive computation and machine learning. MIT Press, Cambridge, Mass., 3. print edition, 2008. ISBN 978-0-262-18253-9.
- Rives, A., Meier, J., Sercu, T., Goyal, S., Lin, Z., Liu, J., Guo, D., Ott, M., Zitnick, C. L., Ma, J., et al. Biological structure and function emerge from scaling unsupervised learning to 250 million protein sequences. *Proceedings of the National Academy of Sciences*, 118(15), 2021.
- Ruffolo, J. A., Gray, J. J., and Sulam, J. Deciphering antibody affinity maturation with language models and weakly supervised learning. *arXiv preprint arXiv:2112.07782*, 2021.
- Schymkowitz, J., Borg, J., Stricher, F., Nys, R., Rousseau, F., and Serrano, L. The foldx web server: an online force field. *Nucleic acids research*, 33(suppl\_2):W382–W388, 2005.
- Shah, A. and Ghahramani, Z. Pareto frontier learning with expensive correlated objectives. In *International Conference on Machine Learning*, pp. 1919–1927. PMLR, 2016.
- Shahriari, B., Bouchard-Côté, A., and Freitas, N. Unbounded bayesian optimization via regularization. In *Artificial intelligence and statistics*, pp. 1168–1176. PMLR, 2016.
- Shrake, A. and Rupley, J. A. Environment and exposure to solvent of protein atoms. lysozyme and insulin. *Journal of molecular biology*, 79(2):351–371, 1973.
- Shu, R., Lee, J., Nakayama, H., and Cho, K. Latent-variable non-autoregressive neural machine translation with deterministic inference using a delta posterior. In *Proceedings of the AAAI Conference on Artificial Intelligence*, volume 34, pp. 8846–8853, 2020.
- Srinivas, N., Krause, A., Kakade, S., and Seeger, M. Gaussian process optimization in the bandit setting: no regret and experimental design. In *Proceedings of the 27th International Conference on International Conference on Machine Learning*, pp. 1015–1022, 2010.

- Tripp, A., Daxberger, E., and Hernández-Lobato, J. M. Sample-efficient optimization in the latent space of deep generative models via weighted retraining. *Advances in Neural Information Processing Systems*, 33, 2020.
- Tripp, A., Simm, G. N., and Hernández-Lobato, J. M. A fresh look at de novo molecular design benchmarks. In *NeurIPS 2021 AI for Science Workshop*, 2021.
- Turner, R., Eriksson, D., McCourt, M., Kiili, J., Laaksonen, E., Xu, Z., and Guyon, I. Bayesian optimization is superior to random search for machine learning hyperparameter tuning: Analysis of the black-box optimization challenge 2020. *arXiv preprint arXiv:2104.10201*, 2021.
- Wang, Z., Hutter, F., Zoghi, M., Matheson, D., and de Feitas, N. Bayesian optimization in a billion dimensions via random embeddings. *Journal of Artificial Intelligence Research*, 55:361–387, 2016.
- Williams, C. K. and Rasmussen, C. E. *Gaussian processes for machine learning*, volume 2. MIT press Cambridge, MA, 2006.
- Wilson, A. G., Hu, Z., Salakhutdinov, R., and Xing, E. P. Deep kernel learning. In *Artificial intelligence and statistics*, pp. 370–378. PMLR, 2016.
- Wu, J., Toscano-Palmerin, S., Frazier, P. I., and Wilson, A. G. Practical multi-fidelity bayesian optimization for hyperparameter tuning. *arXiv pre-print arXiv:1903.04703*, 2019.
- Yang, K. K., Chen, Y., Lee, A., and Yue, Y. Batched stochastic bayesian optimization via combinatorial constraints design. In *The 22nd International Conference on Artificial Intelligence and Statistics*, pp. 3410–3419. PMLR, 2019.
- Zhang, D., Fu, J., Bengio, Y., and Courville, A. Unifying likelihood-free inference with black-box sequence design and beyond. *arXiv preprint arXiv:2110.03372*, 2021.

# Appendices

In Appendix A we outline the three evaluation tasks: **Bigram**, **ZINC**, and **RFP**. In Appendix B, we describe in detail the neural network architecture, the DKL GP implementation, the denoising autoencoder implementation, the string kernel implementation, and the hyperparameters used for our experiments. Finally, in Appendix C, we present additional experimental results to supplement the figures in the main text.

## A. Evaluation Task Details

### A.1. Bigram Task

The bigram task is a simple toy example of discrete sequence optimization. We draw random strings from an alphabet  $\mathcal{V}$  and count the occurrence of  $k$  predetermined bigrams, which we use as proxy fitness targets. The task is to maximize the counts of each bigram in the sequence, restricting the sequence length to 36 tokens (including utility tokens). For our experiments we used the same amino acid vocabulary as our protein task and chose 3 complementary bigrams, “AV”, “VC” and “CA”. The initial sequences were sampled with lengths between 32 and 36 tokens. We ensured there were an equal number of positive examples (sequences with at least one occurrence of one of the bigrams) as negative examples in the starting pool.

### A.2. ZINC Task

The original ZINC logP optimization task, popularized in the BayesOpt community by Gómez-Bombarelli et al. (2018), is to optimize the octanol-water partition coefficient of a small molecule. Molecules with high logP values are hydrophobic and molecules with low values are hydrophilic. Hydrophobicity can be desirable for absorption and solubility, for example in pharmaceuticals. As a property that is easy to calculate, it has risen to prominence despite being undesirable on its own. Very high logP can result in molecules with limited practical application, and moreover finding molecules with high logP reduces trivially to the problem of finding long hydrocarbon chains, as these compounds are extremely hydrophobic relative to the size of the molecule. The *penalized* logP objective adds auxiliary terms measuring synthetic accessibility (Ertl & Schuffenhauer, 2009) and the number of cycles. Unfortunately these terms do not fix the underlying problem, and so penalized logP is similarly vulnerable to optimization hacking, as we discuss in Section 5.5.

Because logP in itself is a deeply flawed objective, both in its relevance to real-world drug design and its ability to be hacked by optimizers, we also consider a multi-objective optimization task that is closer in form to real design problems. Instead of solely optimizing for logP, we jointly optimize for logP and QED (Quantitative Estimate of Druglikeness), a composite metric that captures many elements of druglikeness, with bioavailability among the most prominent (Bickerton et al., 2012). Unfortunately QED has its own limitations as an objective, since it is a simple parametric model trained on a small dataset to emulate heuristics such as Lipinski’s Rule of Five (Lipinski et al., 1997).

The shortcomings of objectives like logP and QED appear to be well-known (Nigam et al., 2019; Tripp et al., 2021; Fu et al., 2020; Maus et al., 2022), but a superior alternative has not yet been accepted by the research community. For example, at the time of writing the only molecule generation benchmark in TorchDrug is maximization of QED and logP of ZINC-like molecules.<sup>2</sup> Angermueller et al. (2020) evaluated BBO algorithms on a substantial number of *in silico* sequence design tasks, however the large molecule tasks they considered were relatively simple, single-objective problems (e.g. maximization of the likelihood of a hidden Markov model). The vacuum of rigorous *in silico* evaluation tasks for large-molecule design motivated us to propose our RFP task as a new benchmark.

We construct the start pool by inverting the scores and selecting the top- $k$  non-dominating sequences (i.e. we found the  $k$  most dominated sequences in the ZINC dataset w.r.t. logP and QED). Constructing the task in this way is better than simply sampling randomly from ZINC because QED is bounded above by 1 and many ZINC sequences already score fairly close to 1. Starting with dominated sequences ensures that there is sufficient headroom for improvement to observe variations in optimizer behavior. We capped the max sequence length at 128 SELFIES tokens, including utility tokens. The SELFIES vocabulary was precomputed from the entire ZINC dataset (Krenn et al., 2020).

<sup>2</sup><https://torchdrug.ai/docs/benchmark/generation.html>

### A.3. RFP Task

In this work we present a new *in silico* benchmark task designed to simulate searching for improved red fluorescent protein (RFP) variants *in vitro*, a problem of significant interest to biomedical researchers (Dance, 2021). We optimize red-spectrum proteins with known structures for stability ( $-dG$  or negative change in Gibbs free energy) and solvent-accessible surface area (SASA) (Shrake & Rupley, 1973; Cock et al., 2009) in simulation, using the FoldX suite (Schymkowitz et al., 2005) and BioPython to evaluate our objective function. Stability as evaluated by FoldX—particularly in the negative case—has been shown to correlate with protein function (Høie et al., 2021). Solvent-accessible surface area will correlate with factors that influence the brightness and photostability of the fluorescent protein: aggregation propensity due to exposed hydrophobic surface (Mishra et al., 2018) and shielding by the beta-barrel, which encapsulates the fluorophore (Chudakov et al., 2010). Since both of these benchmark tasks are functions of the protein’s three-dimensional structure, it is expected that training a model on these tasks will require the model to learn a latent representation for structure, which in turn determines function.

We constructed the start pool in two phases. First we searched FPBase for all red-spectrum (defined in this context as having an emission wavelength at least 580 nm) proteins with at most 244 residues with known 3D structures, selecting the highest resolution structure if more than one was available. If more than one chain was present in the structure, we selected the longest chain as the representative residue sequence. Starting from these base proteins, we used NSGA-2 to collect additional labelled sequences to use in the start pool for subsequent experiments.

Although this task is a significant step forward for *in silico* evaluation of discrete sequence design, it is currently limited by the capabilities of FoldX, which can only compute structures from substitution mutations (i.e. the sequence length cannot change). Deep learning structure oracles such as AlphaFold (Jumper et al., 2021) or RoseTTAFold (Baek et al., 2021) could also be used, but we found FoldX to be simpler and more amenable for rapid prototyping.

## B. Implementation Details

Our models are implemented in PyTorch (Paszke et al., 2019), BoTorch (Balandat et al., 2020), and GPyTorch (Gardner et al., 2018). Our genetic optimizer baselines are implemented in PyMOO (Blank & Deb, 2020). Our code is publicly available at <https://github.com/samuelstanton/lambo>. Hyperparameters are summarized in Appendix B.5.

### B.1. Architecture Details

We used the same base architecture for all experiments, relying on 1D convolutions (masking positions corresponding to padding tokens). We used standard pre-activation residual blocks with two conv layers, layernorm, and swish activations. We used a kernel size of 5, 64 intermediate channels and 16 latent channels.

The shared encoder and decoder each were composed of 3 of these residual blocks (for a total of 6 convolutional layers each). The shared encoder embeds input sequences with standard vocabulary and sinusoidal position embeddings. The discriminative encoder was composed of a single residual block.

Note that transformer encoder layers could be substituted as a drop-in replacement for these convolutional residual blocks, we used small convolutional layers because they are fast to train and performed adequately in our experiments.

### B.2. DKL Implementation Details

Training DKL models is an art. Some best practices apply to both stochastic variational and exact GP inference, others are specific to the former.

#### Applicable to exact and variational GP inference

1. *Kernel hyperparameter priors matter.* Allowing the DKL GP to easily change both the inputs to the final conventional GP kernel (e.g. RBF) and the lengthscale of that kernel doesn’t work well. We placed a tight Gaussian prior ( $\sigma = 0.01$ ) around the initial lengthscale value and forced the encoder to learn features appropriate for that lengthscale. Note that this is distinct from simply fixing the kernel hyperparameters *a priori*.
2. *Optimizer hyperparameters matter.* Adam is really convenient to avoid too much learning rate tuning, but it can cause unexpected issues when jointly training supervised and unsupervised heads. We almost completely disabled the running estimates of the first two moments in Adam, using  $\beta_1 = 0.$ , and  $\beta_2 = 0.01$ .

3. *Normalization matters.* This is more of an issue for SVGPs than exact GPs, but in both cases batchnorm can cause undesirable and unexpected behavior. Use layernorm.

### Applicable to variational GP inference

1. *Initialization matters.* We use the procedure described in Maddox et al. (2021c) to reinitialize the inducing point locations and the variational parameters every time the model was retrained. This trick significantly improves results and saves computation, since the GP training does not completely start over every outer loop iteration.
2. One final trick that is very useful for SVGPs is to turn off gradients to all GP-related parameters every other epoch (so half the epochs are only train the encoder).

As we show in the main text and Figure 9, DKL SVGPs can consistently be trained to similar levels of accuracy as exact DKL GPs with very little trouble, once the proper training procedures are in place. With these practical insights we were able to jointly train supervised GP heads and unsupervised language model heads on a shared encoder simply by taking one gradient step on the supervised GP loss and one gradient step on the unsupervised DAE loss per minibatch, using the same optimizer and learning rate schedule. We used diagonal Gaussian likelihoods for all our experiments, with the noise variance initialized at 0.25.

We found that DKL GPs (both exact and variational) were not immune to overfitting, so we used weight decay ( $1e-4$ ) and reserved 10% of all collected data (including online queries) as validation data for early stopping.

### B.3. DAE Implementation Details

**MLM Head** We used a mask ratio of 0.125 for all experiments when training MLM heads. The MLM loss is computed by randomly masking input tokens, and computing the empirical cross-entropy between the original sequence and the predictive distribution of the MLM head at the masked positions. During sequence optimization the MLM predictive distribution is modified to prevent sampling the original token (to encourage diversity) and to prevent the sampling of special tokens.

**LANMT Head** Our LANMT head is identical to our MLM head, except for the addition of a length prediction head and length transform module (Shu et al., 2020), a different corruption procedure and training objective. We used a max length change of 8 in our experiments for Figure 7, so the corruption function randomly sampled a length change  $\Delta t$  between -8 and 8.  $\Delta t$  tokens were subsequently deleted, replaced, or inserted into the sequence. The corrupted sequence was forwarded through the model, which was also given the original sequence length as a label during training. A training step takes a gradient step on the cross-entropy between the predicted length and the actual length, and on the cross-entropy between the predictive distribution over the whole decoded sequence and the original sequence.

### B.4. SSK Implementation

As we briefly discussed in Section 5.4 in the main text, SSKs have conceptual and practical issues, and empirically do not appear to be exceptionally effective on biological sequence tasks. In fact, SSKs are very similar to  $n$ -gram language models, and have many of the same shortcomings.

**Lack of Positional Information** simply put, an SSK counts the occurrences of every possible  $n$ -gram across every possible combination of tokens in a sequence. The gap decay hyperparameter downweights occurrences corresponding to token combinations that are not closely colocated. Hence SSKs have very limited positional awareness in the sense that sequences with similar  $n$ -gram counts have high prior covariance, regardless of where the  $n$ -grams actually occurred. Positional awareness is important when dealing with biological sequences from some subpopulation (e.g. a family of fluorescent proteins) since they can have many identical subsequences, only varying at key positions that strongly affect function.

**Difficult to Scale** the scaling issues of SSKs primarily have to do with the sequence length, rather than the size of the dataset. The dynamic programming algorithm used by Moss et al. (2020) to compute their SSK is parallelizable, but becomes prohibitively memory intensive for a couple hundred large molecules, even when chunking the sequence into smaller pieces. In fact, we used an Nvidia RTX 8000 GPU with 48 GB of memory to produce Figure 5.4. Methods for scaling GPs to many observations such as random features (Lázaro-Gredilla et al., 2010) or CG-based approaches (Gardner et al., 2018) do not address this issue. Variational GP inference is also impractical because standard variational methods (Hensman et al.,



2013) would place the inducing point locations in the discrete sequence input space, introducing a challenging discrete optimization subproblem just to train the surrogate. We also implemented a memory-efficient trie-based SSK, which could handle longer sequences but was prohibitively slow and difficult to parallelize.

### B.5. Hyperparameters

Sequence Optimization	
Name	Value
$ \mathcal{D}_0 $	512
Query batch size ( $b$ )	16
$ \mathcal{X}_{\text{base}} $	$b$
# Optimization rounds ( $i_{\text{max}}$ )	64
# Inner loop restarts	16
# Inner loop gradient steps ( $j_{\text{max}}$ )	32
Inner loop step size ( $\eta$ )	0.1
Entropy penalty ( $\lambda$ )	1e-2
# MC acquisition samples	2
Random seeds	$\{0, \dots, 9\}$

DAE Architecture	
Name	Value
Shared enc. depth (# residual blocks)	3
Disc. enc. depth (# residual blocks)	1
Decoder depth (# residual blocks)	3
Conv. kernel width (# tokens)	5
# conv. channels	64
Latent dimension	16
GP likelihood variance init	0.25
GP lengthscale prior	$\mathcal{N}(0.7, 0.01)$
# inducing points (SVGP head)	64

DAE Training	
Name	Value
DAE corruption ratio (training)	0.125
DAE learning rate (MTGP head)	5e-3
DAE learning rate (SVGP head)	1e-3
DAE weight decay	1e-4
Adam EMA params ( $\beta_1, \beta_2$ )	(0., 1e-2)
Early stopping holdout ratio	0.1
Early stopping relative tolerance	1e-3
Early stopping patience (# epochs)	32
Max # training epochs	256

## C. Additional Results

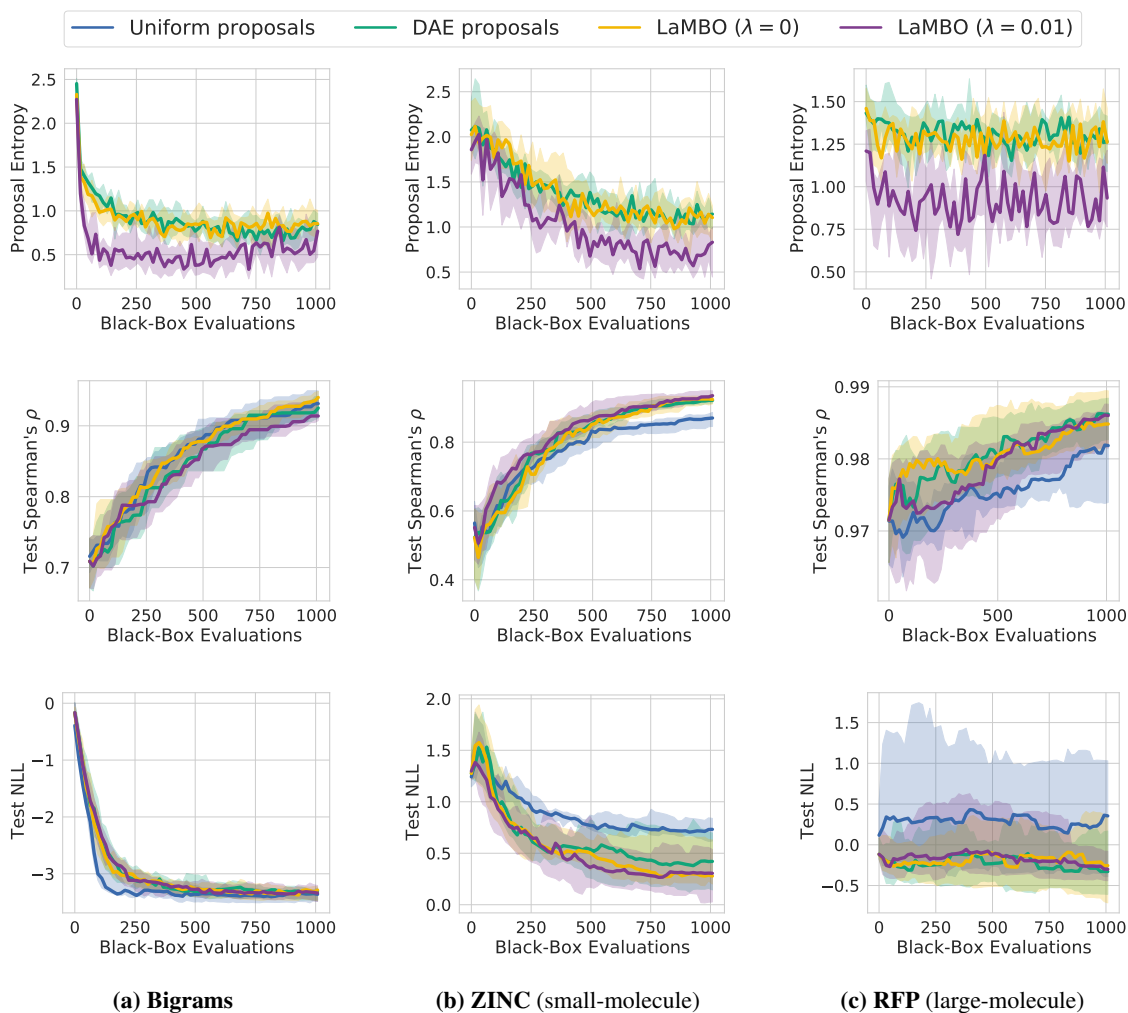


Figure 8. Additional metrics for the ablation experiment described in Section 5.3 and Figure 5, where we cumulatively add the elements described in Section 4.3: (1) DAE-generated proposals, (2) DAE proposal optimization following  $\nabla_Z[\ell_{\text{query}}]$  with  $\lambda = 0$ . (see Eq. (3)), and (3) DAE proposal optimization with  $\lambda = 0.01$ . The **top** row shows the average entropy of the generative DAE proposal distributions over time. As expected, the entropy penalty decreases the proposal entropy. The **middle** and **bottom** rows show the discriminative Spearman's  $\rho$  and NLL (averaged across objectives) on heldout test data over time. Notably, training the LaMBO architecture with both the unsupervised DAE objective and the supervised GP objective improves discriminative performance. The midpoint, lower, and upper bounds of each curve depict the 50%, 20%, and 80% quantiles, estimated from 10 trials.

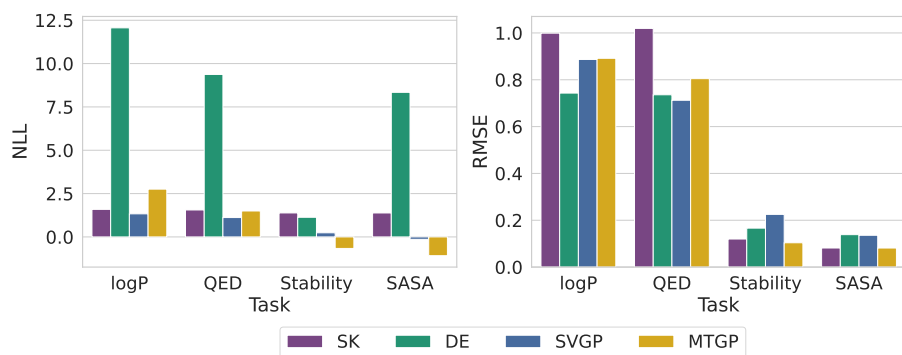


Figure 9. Negative log-likelihood (NLL) and root mean squared error (RMSE) for various discriminative models in the offline regression setting. DKL MTGPs and SVGPs have good performance across the board, while bootstrapped CNN ensembles (DE) are very overconfident. Exact GP inference with a substring kernel (SK) is very underconfident and has poor accuracy when predicting logP and QED.